communications materials

A Nature Portfolio journal

Article

https://doi.org/10.1038/s43246-025-01021-9

Direct to indirect band gap transition induced by approximately dark states

Jiabao Yang[1], Mihir Date[1,2], Irián Sánchez Ramírez[3,4], Vicky Hasse[5], Deepnarayan Biswas[2], Stuart S. P. Parkin[1], Maia G. Vergniory[3,6,7], Fernando de Juan[3,4,8], Claudia Felser[5], Matthew D. Watson[2] & Niels B. M. Schröter[1,9,10]

Recent work suggests that crystal structures with two sublattice pairs per primitive cell can host "dark states", electronic states that barely interact with light due to destructive interference, which makes them invisible in photoemission. In practice, however, dark states are only approximately dark, arising from near but imperfect translation symmetries. Here, we demonstrate a practical consequence of this in the semiconductor $(NbSe_4)_3I$: Although its band structure indicates an almost direct gap, the material behaves optically like an indirect-gap semiconductor. Angle-resolved photoemission spectroscopy uncovers weak spectral-weight bands folded from a larger Brillouin zone, reflecting approximate intra-unit-cell symmetry. These states form a small direct band gap consistent with transport data but exhibit very low optical transition probability. Instead, optical absorption is dominated by higher-energy transitions involving bands with stronger spectral weight, effectively enlarging the observed optical gap. Our results show that dark states are approximate phenomena with significant consequences for optoelectronic properties.

Quantum states that do not allow for optical transitions are often characterized as *dark*[1–3]. A recent publication proposed that such *dark states* generically appear in crystals where two pairs of sublattices are related by a glide symmetry[4], are suggested to result in double destructive interference of electronic wavefunctions, yielding zero probability of electron removal in the spectral function of these dark states, which also excludes optical excitations from them. This work already mentioned potential implications of *dark states* for optoelectronic properties of crystals. However, so far, no concrete example of their influence on the optoelectronic properties of materials has been demonstrated.

Whilst ref. 4 emphasises the importance of glide symmetries for the appearance of dark states, approximate translation symmetry, which generically exist in many materials, are often responsible for the suppression of spectral weight and thus optical transitions[5–12]. It appears when the lowest order terms in a tight binding model allow for translation symmetries involving a small unit cell, but extend to its full primitive size[13] when consider higher order terms. These higher-order corrections result in the emergence of folded bands with weak spectral weight, in addition to bright bands with strong spectral weight, which adhere to the symmetry of the smaller unit cell. Such approximate translation symmetry can explain the suppression of spectral weight in $PdSe_2$ system(See Supplementary Information Section I), as reported in ref. 4. In fact, a complete suppression of folded bands is only possible when the translation symmetry is no longer approximate but the exact symmetries of crystal structure. In this case, the system could be described by a smaller unit cell and thus fewer bands.

In this work, we show that *approximately dark states* that results from approximate translation symmetry can influence optoelectronic properties by redistributing the spectral weight, and thus, cause an almost direct band gap semiconductor $(NbSe_4)_3I$ to behave as if it had an indirect band gap. Transport measurements in this material indicate an activated behaviour with an energy gap that is around 0.2 eV at room temperature[14–19], whereas optical spectroscopy experiments have found an optical gap of at least 0.5 eV[20]. The origin of this discrepancy has so far remained obscure, but could naturally be explained by an effectively indirect band gap. Optical conductivity probes vertical transitions at the same k-point due to negligible photon momentum. In contrast, the transport gap is defined by the energy difference between the valence band maximum and conduction band minimum, which may occur at different k-points. However, our calculations

[1]Max-Planck-Institut für Mikrostrukturphysik, 06120 Halle, Germany. [2]Diamond Light Source Ltd, Harwell Science and Innovation Campus, Didcot, OX11 0DE, UK. [3]Donostia International Physics Center, 20018 Donostia-San Sebastian, Spain. [4]Departamento de Fisica de Materiales, Facultad de Ciencias Quimicas, Universidad del Pais Vasco (UPV-EHU), 20018 Donostia-San Sebastian, Spain. [5]Max Planck Institute for Chemical Physics of Solids, 01187 Dresden, Germany. [6]Département de Physique et Institut Quantique, Université de Sherbrooke, Québec, J1K 2R1 Sherbrooke, Canada. [7]RQMP, Regroupement Québécois sur les Matériaux de Pointe, H3T3J7 Quebec, Canada. [8]IKERBASQUE, Basque Foundation for Science, 48013 Bilbao, Spain. [9]Halle-Berlin-Regensburg Cluster of Excellence CCE, Halle, Germany. [10]Martin-Luther-Universität Halle-Wittenberg, 06120 Halle (Saale), Germany. e-mail: niels.schroeter@mpi-halle.mpg.de

show that the nominal indirect band gap in $(NbSe_4)_3I$ is only 13 meV smaller than the direct band gap, which cannot explain the large discrepancy of almost 300 meV between transport and optical gaps. This discrepancy can only be understood when taking into account the effect of approximately dark states. The optical conductivity depends on the spectral weight, which can be probed by ARPES through the spectral weight distribution of the valence band (See Supplementary Information Section II). While the system is known to exhibit an inversion-symmetry breaking phase transition at 270 K, and some samples show a lower temperature transition around 90 K[21–23], these do not fundamentally alter the apparent disparity between optical and transport gaps.

A recent theoretical study[24] suggests that although the transport band gap is small and almost direct when considering the full primitive unit cell of this material, approximate translation symmetry lead to a strong modulation of the spectral weight, resulting in approximately dark states with vanishing probability of optical excitation across the small transport gap. The optical transitions are instead dominated by bright states with strong spectral weight obeying the symmetry of a smaller unit cell, which results in an enhanced optical band gap compared to the transport gap.

In ARPES measurements, the observable quantity is the one-particle spectral function which contain the relevant spectral weight modulations for the occupied states, from which a lower bound of the band gap can be estimated. However, previous ARPES studies of $(NbSe_4)_3I$ reported a wider band gap, aligning with the value from optics[20,25]. This discrepancy between ARPES and transport results likely occurred because these previous ARPES experiments did not explore the full three-dimensional Brillouin zone of $(NbSe_4)_3I$ due to its alleged one-dimensional nature. In fact, ref. 24 made a specific prediction that to observe the true valence band maximum with full spectral weight, one would need to probe a particular position in momentum space that deviates from the normal emission geometry mainly used in previous ARPES studies[20,25].

Here, by performing photon-energy dependent ARPES measurements, we found that the electronic structure of $(NbSe_4)_3I$ deviates from the previously assumed quasi-1D nature, but instead displays strongly dispersive bands along all three momentum directions. We obtained the electronic band structure along all high-symmetry k paths in a 3D Brillouin corresponding to the smaller unit cell containing only 3-Nb atoms, finding a spectral weight modulation resulting in approximately dark states. Specifically, our data supports a relatively small direct transport gap of 0.2 eV in $(NbSe_4)_3I$ that allows for the thermally activated occupation of approximately dark states which can contribute to transport responses. However, the optical transitions are dominated by the bright states that we also detect in our experiments, and which form an indirect band gap. Beyond the specific example of $(NbSe_4)_3I$, our experiments underline the impact of approximate symmetries on spectroscopic measurements, demonstrating how the presence of approximately dark states lead to an indirect to direct band gap transition which determines the optoelectric properties of semiconductors.

Results and discussion

Crystal structure

The crystal structure of $(NbSe_4)_3I$ is based on $(NbSe_4)$ chains running along the c axis, interspersed with iodine atoms, as shown in Fig. 1a. Along the chain direction, c, in a simplified ionic picture[14] the Nb valence states are sequentially 4+, 4+, 5+, with a shorter bond length for the Nb^{4+}-Nb^{4+} bond (Fig. 2b). This trimerization is already present at room temperature, and is at the heart of understanding why $(NbSe_4)_3I$ exhibit insulating rather than metallic conductivity, which would have been naively expected for $Nb^{4.33+}$ and equal bond lengths[26]. However, the structural unit cell contains not 3 but 12-Nb sites (4 formula units of $(NbSe_4)_3I$) due to the location of the Se and I atoms. Formally, $(NbSe_4)_3I$ belong to the space group $P4/mnc$ (No. 128) at room temperature, which we refer to by its point group symmetry D_{4h} following the convention in ref. 24. There is, however, an approximate translation symmetry shown in Fig. 1c, which is a unit cell with 1/4 the volume and just 3-Nb atoms. The unit cells are related by $c^* = c/2$ and $a^* = a/\sqrt{2}$ (here and throughout, we use the * notation for the approximate 3-Nb unit cell). This would be the repeat unit if only the Nb atoms were considered, and since it is bands of primarily Nb $4d_{3z^2-r^2}$ which dominate the low-energy electronic structure, we can expect this approximate symmetry to play an important role. The orbital parity has been further verified using polarization-dependent measurements, which reveal these states only under LH polarization, whereas they show vanishing spectral weight under LV polarization (See Supplementary Information Section III).

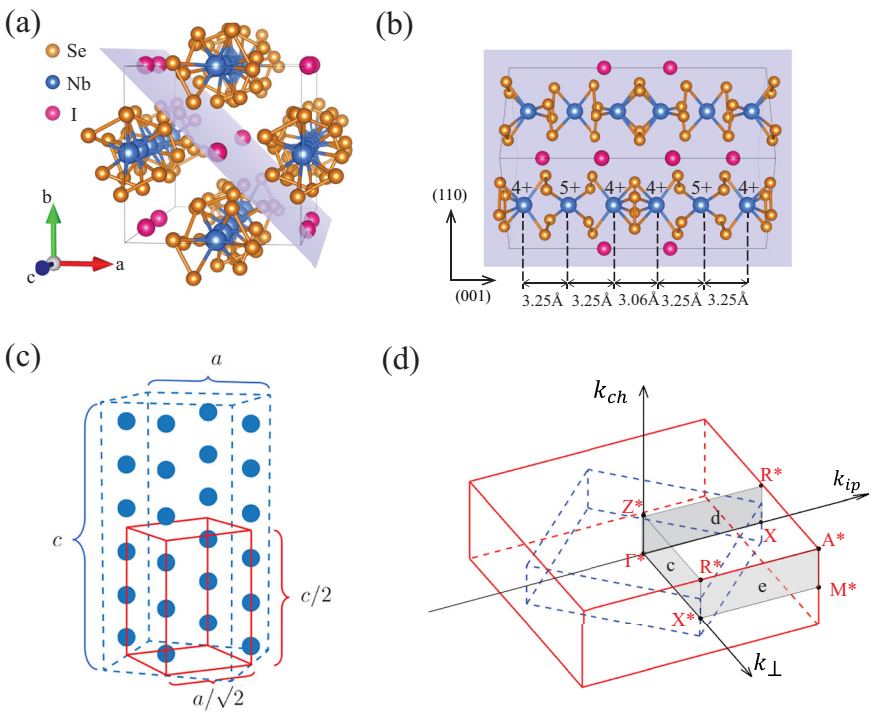

Fig. 1 | Crystal structure and (approximate) Brillouin zone of $(NbSe_4)_3I$. a Side view of the crystal structure and cleavage plane (grey plane). **b** Top view from the (110) cleavage plane. **c** The full 12-Nb unit cell (blue outline) and approximate 3-Nb unit cell (red outline). **d** Brillouin zone derived from (**c**), with high-symmetry points marked with an asterisk (*) to distinguish them from those in the initial 12-Nb unit cell BZ. The grey shaded areas labeled c, d, and e represent the Fermi surface maps, shown later in Fig. 2.

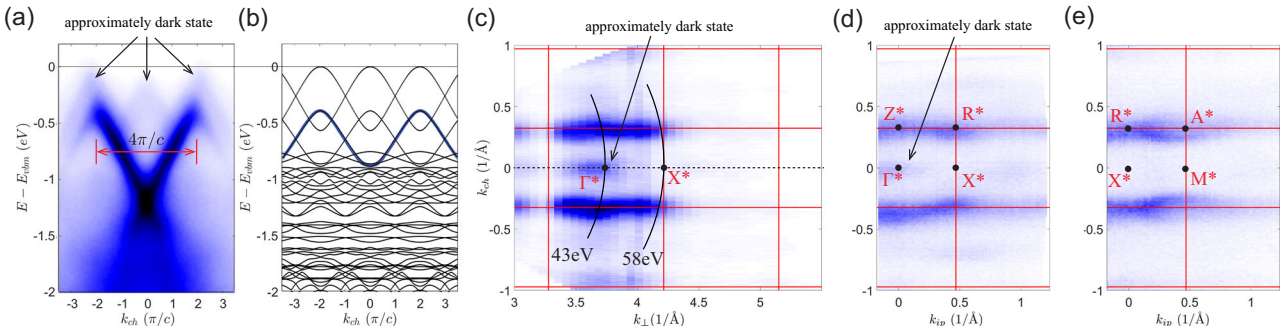

Fig. 2 | Approximately dark states revealed in the dispersion of spectral function along the chain direction. a Dispersion along the chain direction, measured at 43 eV and 90 K. Red arrows indicate the periodicity of $4\pi/c$, and the black arrow points to the approximately dark states. **b** DFT calculation for the 12-Nb-atom structural unit cell. Blue bands correspond to the bright bands observed in (**a**). **c** Photon-energy-dependent iso-energy surface at binding energy $E_b = E_F - 0.3$ eV. The Γ^* and X* points are found at 43 eV and 58 eV, respectively. **d**, **e** Fermi surface maps in the k_{ip} and k_{ch} directions at $h\nu = 43$ eV and $h\nu = 58$ eV, respectively. The binding energy is the same as in (**c**).

In line with literature reports[20], we find that sample cleavage is in the (110) plane, marked with light purple shading in Fig.1. In this geometry, as shown in Fig. 1d we can define k_{ch} as a k-path along the chain, k_{ip} as the direction accessed by in-plane rotation of the analyzer with respect to the sample normal, and $k_\perp$ as the direction normal to the surface. In k-space, the crystallographic 12-Nb BZ is the one marked with dashed blue line in Fig. 1d, but the BZ corresponding to the approximate 3-Nb unit cell is larger and rotated, marked in red. Each of the Γ^*, Z*, M*, A* points map to Γ points of the crystallographic unit cell.

Approximately dark states in ARPES

In the ARPES dispersion along the chain direction, k_{ch}, presented in Fig. 2a, one notable feature is that the spectral weight is dominated by a "bright band". The maximum of the bright band is found at 0.5 eV below E_F, and the separation between these features, i.e., the periodicity of the bright band, is found to be $4\pi/c$. Thus, the brightest features in the data seem to follow the expected periodicity for the approximate 3-Nb unit cell, not the crystallographic 12-Nb one. The data bears similarity to the older literature reports, albeit that the valence band maximum of the main band in the literature was found at somewhat higher binding energies[20,25].

As well as the bright band, approximately dark states above −0.5 eV are also observed in Fig. 2a, marked by the black arrow. This indicates the 12-Nb unit cell must be considered for identifying all states within the measured spectral function, and so careful understanding of the interplay of the crystallographic and approximate unit cells is required. Fig. 2b shows the DFT calculation for the D_{4h} phase. The low energy bands stem from Nb $4d_z^2$ orbitals and have cosine-like dispersions along k_{ch}. Although the band structure overall has a periodicity of $2\pi/c$ in the calculations, as is required from the crystallographic reciprocal lattice, each of the cosine-like bands has a periodicity of $4\pi/c$, or $2\pi/c^*$, following the periodicity of this approximate 3-Nb unit cell. The presence of multiple copies of these cosine-like dispersions derives from the combination of finite hopping transverse to the chains, together with the expansion of the unit cell compared with the approximate 3-Nb description. However, it is clear that only one of these branches in the calculation is "bright" experimentally, while the three other branches are the approximately dark states. Conceptually, in the 3-Nb unit cell there would be a single band dispersing upwards along k_{ch} from a minimum at Γ^*, but due to the higher order hopping terms which break this symmetry, some much weaker spectral weight is found on the approximately dark states.

To investigate the hopping perpendicular to the chains, we need to understand the dispersion along $k_\perp$ and k_{ip} as well as k_{ch}. In our ARPES setup, the $k_\perp$ is accessible by tuning the photon energy according to the nearly free electron final state approximation[27]. After performing such a mapping from $h\nu$, we show in Fig. 2c the spectral weight as a function of $k_\perp$ at an energy of $E - E_F = -0.3$ eV. Here the intensity variations are due to photon energy-dependent cross-sections combined with the beamline characteristics, and thus the spectral weight variation should not be over-interpreted, but the feature that can be consistently identified is the "bright band", which shows a clear warping at with a "neck" in the X* point plane and a "belly" in the Γ^* plane. This warping is a clear indication of significant interchain hopping. The periodicity of the dispersion of the bright band along $k_\perp$ again matches the expected periodicity for the 3-Nb approximate unit cell, as indicated by the red Brillouin zone drawn.

In the D_{4h} phase, k_{ip}, accessed by varying the emission angle between the sample and the analyzer, is symmetry-equivalent to the $k_\perp$. Having established the high symmetry planes from the $k_\perp$ dispersion at normal emission, in-plane k_{ip}-k_{ch} constant energy maps allow us to access all the high symmetry points of the approximate 3-Nb unit cell. The two experimental planes shown in Fig. 2d–e, at 43 eV and 58 eV respectively, are also marked as grey shaded areas in Fig 1d. Again, the periodicity of the bright band with k_{ip} also follows the 3-Nb unit cell, while the warping again highlights the interchain hopping.

Since the ARPES spectral weight principally follows the 3-Nb approximate cell description, in Fig. 3, we directly compare the ARPES data with DFT calculations including a spectral weight factor from an "unfolding" procedure onto the effective 3-Nb unit cell, as described in ref. 24. All the high symmetry points of the chosen k path (except R*) map to Γ^* in the structural unit cell, but clearly the spectral weight varies dramatically, and in the occupied states mainly follows a single "bright band", as seen also in our ARPES results. By interpolating the data from the two k_{ip}-k_{ch} maps shown in Fig. 2d–e, connected at the R* point which is common to both, we construct the ARPES dispersion along the equivalent k path. The distribution of spectral weight agrees well with the calculation, and particularly highlights that the band maximum of the "bright band" in the 3D Brillouin zone is found at the A* point. The A* point can only be accessed experimentally by the correct combination of $k_\perp$ and k_{ch}, a subtlety which was not appreciated in previous ARPES reports.

We note that long-term temperature-dependent measurements may not be feasible due to the thermally activated loss of iodine from the surface, which was previously observed in $(TaSe_4)_2I$[28], while sample charging may occur at lower temperatures. As a result, alternative probes are likely better suited for investigating the temperature evolution of the gap[26]. Our measurements were performed at 90 K, which corresponds to the D_{2h} phase[14]. To verify our results, we conducted charging tests during the measurements and confirmed that the sample did not suffer from charging initially; however, the intensity of the iodine core levels decreased significantly at later stages. We also repeated the measurements to check whether the approximately dark and bright states remained visible, and indeed they did (See Supplementary Information Section IV).

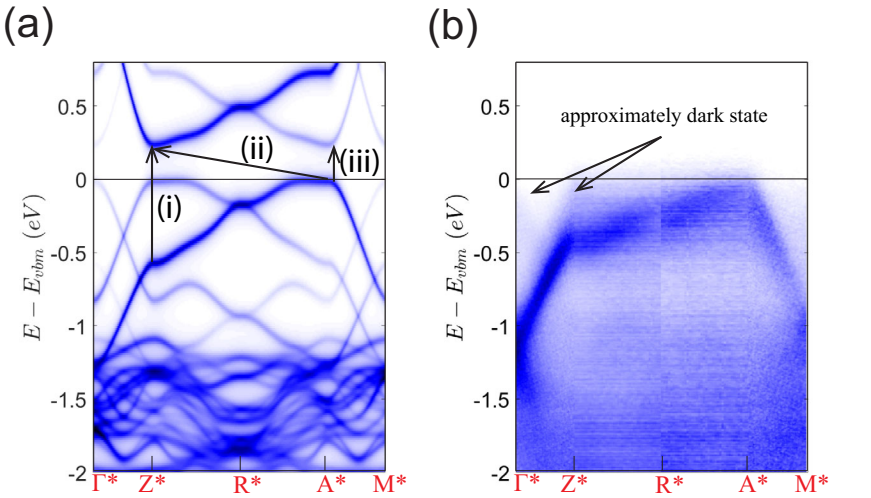

Fig. 3 | Comparison between DFT calculation and ARPES results reveals bright and dark states. **a** DFT calculation with unfolded spectral function. The physical crystal structure with 12 Nb atoms are interpreted as a periodically with 3-Nb atoms. Three distinct gaps have been identified: (i) a direct band optical band gap from bright state to bright state, (ii) indirect electron band gap from bright state to bright state (iii) direct band gap from the bright state to approximately dark state. **b** ARPES dispersion along the equivalent k path. Black arrows indicate approximately dark states.

Nevertheless, we emphasize that we probed bulk-like states in our measurements, and therefore the main conclusions remain valid irrespective of the space group, since the D_{2h} phase also possesses a 12-Nb unit cell.

Discussion

The data plotted in Fig. 3 shows that the band structure of $(NbSe_4)_3I$ is very close to an optical direct band gap(at least 0.5eV) at the Z^* points, labeled with process(i). However, due to the spectral weight modulation of the approximately dark states that we clearly detect in our ARPES experiment, the optical properties are rather dominated by transitions between bands at higher energies with larger spectral weight, so that $(NbSe_4)_3I$ effectively behave as an indirect band gap semiconductor in optics, with the transition from valence band at A^* points to the conduction band at Z^* point. The observed gap size of ~ 0.2 eV aligns with transport measurements, labeled with progress(ii). The direct band gap to indirect band gap transition is introduced by the presence of approximately dark states.

This behavior stems from the presence of approximate symmetries in the electronic structure, which effectively suppress the spectral weight of certain bands in both ARPES and optical measurements. Our use of the term approximately dark states is motivated by this suppression, which reflects the persistence of symmetry constraints that are not exact, but still exert significant influence on the observable spectral features. These findings align with recent theoretical work[13,29], which shows that tight-binding models with restricted hopping can exhibit enhanced or emergent symmetries not apparent in the underlying crystal structure. Our results demonstrate that such quasi-symmetries have tangible consequences for experimental observables, such as deviations between optical and transport gaps even in materials that would be considered direct band gap materials when not considering the effect of approximate symmetries.

This interesting behaviour may occur more generally as long as both conduction and valence bands derive from the same orbital and Wyckoff position in the unit cell, so that the same approximate translation symmetry apply to both. It is also worth noting that even if the folding perturbation does not align conduction and valence band edges, it will still be the case that the optical and transport responses will generally be different, although the true gap will not be direct in that case. If conduction and valence bands derive from different orbitals or Wyckoff positions, then it may be that only one of them shows the dark state modulation, or that such modulation is different for each, and the near-vanishing of optical matrix elements is generally lost.

Conclusion

In conclusion, our work showcases a simple but dramatic example of how approximately dark states may impact the optoelectronic properties of a system and lead to glaring discrepancies with other experimental probes such as transport. These discrepancies are nevertheless readily understood by mapping out the dark bands spectral weight in an ARPES experiment, which we hope may serve to address similar problems in other materials beyond $(NbSe_4)_3I$.

Methodology

Sample growth

The single crystals of $(NbSe_4)_3I$ were grown by chemical vapour transport. The single crystals were synthesised by stoichiometric niobium (Nb, powder, Alfa-Aesar, 99.8%), selenium (Se, Alfa-Aesar, 99.999%) and iodine with the transport agent iodine sealed in an evacuated fused silica ampoule at 500 °C for 7 days. After the reaction, the ampoule was removed from the furnace and quenched in water. The needle crystals were characterised by powder XRD (Huber Guinier G670).

ARPES measurements

The ARPES measurements were performed at the nano-branch of the I05 Beamline at the Diamond Light Source Ltd, UK[30] using linear horizontal (LH) polarized vacuum UV (VUV) radiation. Capillary mirror optics were used to obtain a micro-focused beamspot of approximately 4 µm. Our samples were cleaved in situ and measured at a temperature of 90 K, and pressure less than 2×10^{-10}mbar using a Scienta DA30 analyzer with combined resolution of around 25 meV. The band structure along the $k_\perp$ momentum direction was measured by varying the photon energy between 27 eV and 108 eV, at normal emission. From these measurements, the photon energy corresponding to the Γ^* and X^* planes was determined to be 43 eV and 58 eV, respectively. The Fermi level in Fig. 1(c) was determined by measuring the photoemission signal from a gold sample, with the same photon and pass energy. The valence band maximum in Fig. 3b was aligned to the Fermi level (E_F) by fitting the energy dispersive curve (EDC) with the Fermi-Dirac distribution at A^* point. The intensity was normalized to the main band measured at 43 eV.

Density function theory

Density functional theory (DFT) calculations of the band structures were performed using VASP[31,32] v.6.2.1 with projector-augmented wave pseudopotentials and Perdew Burke Ernzerhof (PBE) parametrization[33]. Self-consistent calculations considering spin-orbit coupling were found to be well converged for a kinetic energy cutoff of 520 eV and a $9 \times 9 \times 5$ k-mesh sampling.

The left-hand side from Fig. 3 in the main text was generated following the method of unfolding by Popescu and Zunger[34] as implemented in VaspBandUnfolding package[35].

Data availability

After acceptance of the manuscript, we will upload all the source data to the Open Research Data Repository of the Max Planck Society, and a DOI will be posted https://edmond.mpg.de/. All the data used for generating the figures for this work have been deposited in the Open Research Data Repository of the Max Planck Society EDMOND. https://doi.org/10.17617/3.8FOBM8.

Received: 22 June 2025; Accepted: 11 November 2025;
Published online: 29 November 2025

References

1. Fleischhauer, M., Imamoglu, A. & Marangos, J. P. Electromagnetically induced transparency: optics in coherent media. *Rev. Mod. Phys.* **77**, 633–673 (2005).
2. Na, M. X. & Ye, Z. Probing the dark side of the exciton. *Science* **370**, 1166–1167 (2020).
3. Ye, Z. L. et al. Probing excitonic dark states in single-layer tungsten disulphide. *Nature* **513**, 214–218 (2014).
4. Chung, Y. et al. Dark states of electrons in a quantum system with two pairs of sublattices. *Nat. Phys.* **20**, 1582–1588 (2024).
5. Daimon, H., Imada, S., Nishimoto, H. & Suga, S. Structure factor in photoemission from valence band. *J. Electron Spectrosc. Relat. Phenom.* **76**, 487–492 (1995).
6. Matsui, F., Matsushita, T. & Daimon, H. Photoelectron structure factor and diffraction spectroscopy. *J. Electron Spectrosc. Relat. Phenom.* **195**, 347–360 (2014).
7. Shirley, E. L., Terminello, L., Santoni, A. & Himpsel, F. Brillouin-zone-selection effects in graphite photoelectron angular distributions. *Phys. Rev. B* **51**, 13614 (1995).
8. Mucha-Kruczyński, M. et al. Characterization of graphene through anisotropy of constant-energy maps in angle-resolved photoemission. *Phys. Rev. B-Condens. Matter Mater. Phys.* **77**, 195403 (2008).
9. Liu, Y., Bian, G., Miller, T. & Chiang, T.-C. Visualizing electronic chirality and Berry phases in graphene systems using photoemission with circularly polarized light. *Phys. Rev. Lett.* **107**, 166803 (2011).
10. Hwang, C. et al. Direct measurement of quantum phases in graphene via photoemission spectroscopy. *Phys. Rev. B-Condens. Matter Mater. Phys.* **84**, 125422 (2011).
11. Jung, S. W. et al. Black phosphorus as a bipolar pseudospin semiconductor. *Nat. Mater.* **19**, 277–281 (2020).
12. Brouet, V. et al. Impact of the two fe unit cell on the electronic structure measured by ARPES in iron pnictides. *Phys. Rev. B-Condens. Matter Mater. Phys.* **86**, 075123 (2012).
13. Dagnino, A. et al. The landscape of symmetry enhancement in tight-binding models. *arXiv preprint arXiv:2409.02999* (2024).
14. Gressier, P., Meerschaut, A., Guemas, L., Rouxel, J. & Monceau, P. Characterization of the new series of quasi one-dimensional compounds $(MX_4)_nY$ (m= Nb, Ta; x= S, Se; Y= Br, I). *J. Solid State Chem.* **51**, 141–151 (1984).
15. Taguchi, I., Levy, F. & Berger, H. Metal-insulator transitions in the quasi-one-dimensional compound $(NbSe_4)_3I$. In *Proceedings of the Yamada Conference XV on Physics and Chemistry of Quasi One-Dimensional Conductors* 258–260 (Elsevier, 1986).
16. Gressier, P., Guemas, L. & Meerschaut, A. (NbSe4) 3i low temperature structure. *Mater. Res. Bull.* **20**, 539–548 (1985).
17. Taguchi, I., Lévy, F. & Berger, H. Observation of nonlinear conduction in $(NbSe_4)_3I$. *Jpn. J. Appl. Phys.* **26**, 619 (1987).
18. Izumi, M. et al. Evidence of a phase transition in a new type of halogenated niobium tetraselenide $(NbSe_4)_xI$. *Solid State Commun.* **49**, 423–426 (1984).
19. Smontara, A., Biljaković, K., Forró, L. & Levý, F. Properties of the phase transition in $(NbSe_4)_3I$. *Phys. B++ C.* **143**, 264–266 (1986).
20. Vescoli, V. et al. Dynamical properties of the one-dimensional band insulator $(NbSe_4)_3I$. *Phys. Rev. Lett.* **84**, 1272–1275 (2000).
21. Sekine, T., Izumi, M. & Matsuura, E. Raman scattering in linear-chain compounds $(NbSe_4)_{\frac{10}{13}}I$ and $(NbSe_4)_3I$. *Synth. Met.* **19**, 869–874 (1987).
22. Ikari, T. & Lévy, F. Raman spectra of $(NbSe_4)_3I$ and $(TaSe_4)_2I$ single crystals. *J. Phys. C Solid State Phys.* **18**, L1109 (1985).
23. Sekine, T. & Izumi, M. Successive phase transitions in the linear-chain semiconductor $(NbSe_4)_3I$ studied by Raman scattering and electrical resistivity. *Phys. Rev. B* **38**, 2012 (1988).
24. Sánchez-Ramírez, I., Vergniory, M. G., Felser, C. & de Juan, F. Band structures of $(NbSe_4)_3I$ and $(TaSe_4)_3I$: reconciling transport, optics, and angle-resolved photoemission spectroscopy. *Phys. Rev. B* **107**, 205109 (2023).
25. Grioni, M. et al. The spectroscopic properties of 1D Peierls systems. *J. Electron Spectrosc. Relat. Phenom.* **114**, 653–657 (2001).
26. Dominko, D. et al. Static and dynamic properties of low-temperature order in the one-dimensional semiconductor $(NbSe_4)_3I$. *Phys. Rev. B* **94**, 104113 (2016).
27. Damascelli, A. Probing the electronic structure of complex systems by ARPES. *Phys. Scr.* **2004**, 61 (2004).
28. Yi, H. et al. Surface charge induced dirac band splitting in a charge density wave material $(TaSe_4)_2I$. *Phys. Rev. Res.* **3**, 013271 (2021).
29. Gohlke, M., Corticelli, A., Moessner, R., McClarty, P. A. & Mook, A. Spurious symmetry enhancement in linear spin wave theory and interaction-induced topology in magnons. *Phys. Rev. Lett.* **131**, 186702 (2023).
30. Hoesch, M. et al. A facility for the analysis of the electronic structures of solids and their surfaces by synchrotron radiation photoelectron spectroscopy. *Rev. Sci. Instrum.* **88**, 013106 (2017).
31. Kresse, G. & Furthmüller, J. Efficient iterative schemes for ab initio total-energy calculations using a plane-wave basis set. *Phys. Rev. B* **54**, 11169 (1996).
32. Kresse, G. & Furthmüller, J. Efficiency of ab-initio total energy calculations for metals and semiconductors using a plane-wave basis set. *Comput. Mater. Sci.* **6**, 15–50 (1996).
33. Perdew, J. P., Burke, K. & Ernzerhof, M. Generalized gradient approximation made simple. *Phys. Rev. Lett.* **77**, 3865 (1996).
34. Popescu, V. & Zunger, A. Extracting e versus k effective band structure from supercell calculations on alloys and impurities. *Phys. Rev. B-Condens. Matter Mater. Phys.* **85**, 085201 (2012).
35. Qijing, Z., Ionizing, Hongkee, Y. & Boyoung, Z. *VaspBandUnfolding* https://github.com/QijingZheng/VaspBandUnfolding.git.

Acknowledgements

We acknowledge Diamond Light Source for time on Beam-line I05 under Proposal No. SI33319. N.B.M.S. was funded by the European Union (ERC Starting Grant ChiralTopMat, project number 101117424).

Author contributions

J.Y. analyzed the data, M.D., D.B., and M.D.W. performed ARPES measurements. I.S.R., M.G.V., and F.J. performed the DFT calculation. C.F. and V.H. grew the crystals. N.B.M.S., F.J., M.D.W. and S.S.P.P. supervised parts of the project. J.Y., M.D.W., and N.B.M.S. wrote the manuscript with contribution from all authors.

Funding
Open Access funding enabled and organized by Projekt DEAL.

Competing interests
The authors declare no competing interests.

Additional information
Supplementary information The online version contains supplementary material available at https://doi.org/10.1038/s43246-025-01021-9.

Correspondence and requests for materials should be addressed to Niels B. M. Schröter.

Peer review information *Communications Materials* thanks the anonymous reviewers for their contribution to the peer review of this work.